crystals

MDPI

Article

A Rare Structural Motif for a Luminescent Cu(I) Coordination Polymer with 3-(Pyridin-2-yl)triimidazotriazine

Daniele Malpicci [1,2], Delia Blasi [1], Daniele Marinotto [2,3], Alessandra Forni [2,3,*], Elena Cariati [1,2,3], Elena Lucenti [2,3] and Lucia Carlucci [1,3,*]

[1] Department of Chemistry, Università degli Studi di Milano, Via Golgi 19, 20133 Milano, Italy
[2] Institute of Chemical Sciences and Technologies "Giulio Natta" (SCITEC) of CNR, Via Golgi 19, 20133 Milano, Italy
[3] INSTM Research Unit of Milano, Via Golgi 19, 20133 Milano, Italy
* Correspondence: alessandra.forni@scitec.cnr.it (A.F.); lucia.carlucci@unimi.it (L.C.)

Abstract: The coordination ability of the pyridine derivative of cyclic triimidazole, namely 3-(pyridin-2-yl)triimidazotriazine (**TT-Py**) towards Cu(I) was explored. **TT-Py** is an appealing nitrogen-rich ligand characterized by the presence of three imidazole nitrogen atoms with trigonal symmetry and a pyridine moiety, available for coordination to metal ions. The multidentate nature of **TT-Py** allows to isolate, by reaction with CuI at room temperature, the one-dimensional coordination network $[Cu_2I_2(TT\text{-}Py)]_n$ (**1**). **1** is characterized by a rare structural network built-up by the combination in a 1:2 ratio of two common motifs for Cu(I) halides coordination polymers, which are the double-stranded stair and the zig-zag chain. **1** displays one broad long-lived emission in the solid state, which has been associated, by the support of DFT and TDDFT calculation, with low-energy transitions of MLCT or XMLCT character.

Keywords: Cu coordination polymers; Cu(I) halides; photoluminescence; N-ligand

check for updates

Citation: Malpicci, D.; Blasi, D.; Marinotto, D.; Forni, A.; Cariati, E.; Lucenti, E.; Carlucci, L. A Rare Structural Motif for a Luminescent Cu(I) Coordination Polymer with 3-(Pyridin-2-yl)triimidazotriazine. *Crystals* **2023**, *13*, 149. https://doi.org/10.3390/cryst13010149

Academic Editors: Ileana Dragutan, Fu Ding, Ya-Guang Sun and Valerian Dragutan

Received: 21 December 2022
Revised: 10 January 2023
Accepted: 13 January 2023
Published: 14 January 2023

Copyright: © 2023 by the authors. Licensee MDPI, Basel, Switzerland. This article is an open access article distributed under the terms and conditions of the Creative Commons Attribution (CC BY) license (https://creativecommons.org/licenses/by/4.0/).

1. Introduction

Coordination compounds of monovalent d^{10} metals, such as Cu(I), Ag(I) and Au(I), are receiving increasing attention due to their fundamental emissive properties, which allow their applications in diverse areas spanning from light-emitting devices to biological sensors [1–9]. In particular, thanks to their usually high quantum efficiency, low-cost and high natural abundance, Cu(I) coordination compounds are the most investigated and appealing among the d^{10} metal series. The incredibly rich structural diversity of Cu(I) derivatives and their structural dependent luminescence have urged the search for new systems to clarify the emissive mechanisms in view of optimizing their performances [10].

The photoluminescent behavior of Cu(I) derivatives has been associated to a combination of metal-to-ligand charge transfer (MLCT), halide-to-metal charge transfer (XLCT) and cuprophilic interactions, often leading to thermochromism, vapochromism and mechanochromism [3,11]. Cu(I) ions generally coordinate with nitrogen-, sulfur- and phosphorus-containing ligands (N-, S- and P-ligands, respectively) [12,13]. Among them, structures with monodentate or multidentate N-ligands are the most common ones, often showing intriguing luminescent properties and structural motifs spanning from one-dimensional (1D) to three-dimensional (3D) networks [10,14–21].

In recent years, our research group has been involved in the synthesis and photophysical characterization of triimidazo[1,2-*a*:1′,2′-*c*:1″,2″-*e*][1,3,5]triazine, hereafter **TT**, and its derivatives. **TT** is a flat nitrogen-rich organic molecule displaying crystallization-induced emission (CIE) and room temperature ultralong phosphorescence (RTUP) with lifetimes up to 1 s at ambient conditions. Such phenomena have been ascribed to the presence of H-aggregates in the solid state, as supported by X-ray diffraction studies, theoretical calculations and previous literature [22,23]. Intriguingly, the presence of three exo-oriented

nitrogen atoms with trigonal symmetry, all available for coordination to metal ions, has paved the way to the use of **TT** as a versatile ligand for the preparation of metal complexes and coordination polymers (CPs) [24–28]. In particular, we previously reported detailed investigations on the synthesis and structural characterization of a family of isostructural Ag(I) and Cu(I) CPs, comprising 1D chains (**[MI(TT)]**$_n$, M = Cu, Ag) and 3D networks (**[MCl(TT)]**$_n$) displaying excitation dependent photoluminescence [27]. DFT/TDDFT calculations and analysis of the X-ray crystal structures allowed to establish that emission from the Ag(I) compounds has mostly a ligand-centered nature, while the isostructural Cu(I) compounds show non-thermally equilibrated XMLCT and ligand-centered emissive states. This difference in the emissive behavior of Ag(I) and Cu(I) compounds has been explained by performing a QTAIM topological analysis of electron density, disclosing a higher shell-shared character of the Cu–N bond with respect to the Ag–N one [29].

Functionalization of **TT** with a pyridinic fragment seemed very interesting both in view of modifying the photophysical features of the triimidazolic scaffold itself and to verify its metal coordination ability when complemented with an additional nitrogen atom, which can increase its versatility in assembling CPs. In this regard, we have already reported the synthesis and photophysical behavior of 3-(pyridin-2-yl)triimidazotriazine (**TT-Py**), in which the nitrogen atom of the pyridine moiety is in an ortho position with respect to **TT** [30]. The ortho substitution allows the possibility of different metastable states, resulting in the isolation of three polymorphs in the crystalline phase and in a peculiar photophysical behavior in the aggregated phase. In fact, **TT-Py** displays excitation-dependent emission covering the entire visible region and comprising dual fluorescence and multiple RTPs even in blended films [30]. On the other side, the coordination ability of **TT-Py** was verified by reaction with Cu(II) salts, resulting in non-emissive dinuclear **[Cu$_2$(CH$_3$COO)$_4$(TT-Py)$_2$]** and in 1D coordination polymer **[Cu(NO$_3$)$_2$(TT-Py)]**$_n$. In **[Cu$_2$(CH$_3$COO)$_4$(TT-Py)$_2$]**, **TT-Py** coordinates as a monodentate through the triimidazole N-binding site most distant to the pyridine substituent, while in **[Cu(NO$_3$)$_2$(TT-Py)]**$_n$, it chelates through the pyridine and one imidazole nitrogen atom, forming a seven-membered metallacycle [28].

In the present work, by reaction of copper iodide with **TT-Py** in CH_3CN at room temperature, a new emissive Cu(I) CP, namely **[Cu$_2$I$_2$(TT-Py)]**$_n$ (**1**), characterized by a rare crystal structure motif, comprising a double-stranded $(CuI)_2$ stair and a single CuI zig-zag chain, was obtained. The photophysical behavior of **1** was investigated, revealing a long-lived emission that, based on DFT-TDDFT calculations, is associated with low-energy transitions of MLCT or XMLCT character.

2. Materials and Methods

All the reagents were purchased from chemical suppliers and used without further purification unless otherwise stated. CuI was purified via dissolution in a saturated aqueous solution of KI and further precipitation with water. 3-(pyridin-2-yl)triimidazotriazine (**TT-Py**) was prepared by Stille coupling between 3-bromotriimidazotriazine and 2-(tributylstannyl)pyridine as reported elsewhere [30]. Thermogravimetric analysis (TGA) was acquired using a Perkin–Elmer TGA 7 instrument under dynamic nitrogen flow (10 mL/min). Powder X-ray diffraction patterns (PXRD) were recorded on a Rigaku Miniflex diffractometer (Cu *K*α radiation, λ = 1.5405 Å) in the 5–55° 2θ range (0.015° and 1 s per step). Elemental analysis was carried out at the microanalytical laboratory of the University of Milan with a Perkin–Elmer 2400 instrument.

2.1. Synthesis of ***[Cu$_2$I$_2$(TT-Py)]$_n$ (1)***

5 mL of a CH_3CN solution of CuI (110 mg, 0.58 mmol) was slowly added to **TT-Py** (80 mg, 0.29 mmol) dissolved in 5 mL of CH_3CN. Few minutes after mixing, the initial precipitation of a microcrystalline yellow powder was observed. The mixture was left to react under stirring at room temperature for 3 h. The solid was recovered by filtration on a Teflon membrane (0.2 µm), washed with 5 mL of CH_3CN and dried in air to give pure **1** (126 mg, 65% yield).

Needle-shaped yellow crystals of **1**, suitable for single crystal X-ray diffraction analysis, were isolated at room temperature by slow diffusion of a CH_3CN solution of CuI into a solution of **TT-Py** in the same solvent.

Elem. anal.: calc. for $C_{14}H_9Cu_2I_2N_7$ (%): C = 25.63, H = 1.38, N = 14.94 found (%): C = 26.35, H = 1.53, N = 15.38.

2.2. Crystal Structure Analysis

Single-crystal X-ray diffraction data for **1** were collected at room temperature on a Bruker APEX II CCD area detector diffractometer, using graphite-monochromated Mo Kα radiation (λ = 0.71073 Å). A full sphere of reciprocal space was scanned by 0.5° ω steps, collecting 2160 frames in six different regions of the reciprocal space. After integration, an empirical absorption correction was made on the basis of the symmetry-equivalent reflection intensities measured [31]. The dataset was truncated at 0.8 Å resolution as a consequence of the poor diffraction quality of the specimen.

The structure was solved by direct methods (SIR 2014 [32]) and subsequent Fourier synthesis; it was refined by full-matrix least-squares on F^2 (SHELX 2014 [33]) using all the reflections. Weights were assigned to individual observations according to the formula $w = 1/[\sigma^2(F_o^2) + (aP)^2 + bP]$, where $P = (F_o^2 + 2F_c^2)/3$; a and b were chosen to give a flat analysis of variance in terms of F_o^2. Anisotropic parameters were assigned to all the non-hydrogen atoms. All the hydrogen atoms were placed in an idealized position and refined riding on their parent atom with an isotropic displacement parameter 1.2 times that of the pertinent parent atom.

The final difference electron density map showed no features of chemical significance, with the largest peaks lying close to the iodine atoms.

Crystal data, data collection and refinement details of the structural analyses are summarized in Table S1, while a selection of geometric parameters are collected in Table S2. CCDC 2227043 contain the supplementary crystallographic data for **1** (see supplementary materials). These data can be obtained free of charge via http://www.ccdc.cam.ac.uk/conts/retrieving.html accessed on 16 December 2022, or from the Cambridge Crystallographic Data Centre, 12 Union Road, Cambridge CB2 1EZ, UK; fax: (+44) 1223-336-033; or e-mail: deposit@ccdc.cam.ac.uk.

2.3. Theoretical Methods

Computational studies were performed on a discrete model of **1**, comprising a central $(CuI)_4$ double strand, two lateral single zig-zag $(CuI)_2$ chains and four bridging ligands (see Figure S5), using the Gaussian 16 suite of programs [34]. Its geometry was optimized with proper constraints (see below) at the ωB97X/6-311++G(d,p) levels of theory, starting from the fragment extracted from the X-ray crystal structure. The all-electron basis set for iodine was downloaded from the Basis Set Exchange site [35–37] with the exponents of the s and p diffuse functions taken from the literature [38]. The ωB97X functional [39] was chosen in view of its optimal performance in treating the geometrical and electronic features of **TT** derivatives [23–30,40–46], including π-π interactions that play an important role in the photophysics of the present structures. Geometry optimization was performed by freezing angles and torsions to preserve the correct coordination geometry around the metal ions. The optimized distances are generally rather close to the experimental values (see Table S3), though the symmetry of the infinite polymeric chain is lost owing to major boundary effects. TDDFT calculations were performed at the ωB97X/6-311++G(d,p) level of theory. Importantly, we adopted here the same computational protocol previously used to model the **[CuI(TT)]$_n$** CP [27,29], allowing to make meaningful comparisons between the electronic properties of the two compounds.

2.4. Photophysical Characterization

Photoluminescence quantum yields were measured using a C11347 Quantaurus–Absolute Photoluminescence Quantum Yield Spectrometer (Hamamatsu Photonics K.K,

Shizuoka, Japan), equipped with a 150 W Xenon lamp, an integrating sphere and a multichannel detector. Steady-state emission and excitation spectra and photoluminescence lifetimes were obtained using a FLS 980 (Edinburg Instrument Ltd., Livingston, UK) spectrofluorimeter. The steady-state measurements were recorded by a 450 W Xenon arc lamp. Photoluminescence lifetime measurements were performed using an Edinburgh Picosecond pulsed diode laser (emitted wavelength 374 nm) and microsecond flash Xe-lamp (60 W, 0.1 ÷ 100 Hz) with data acquisition devices time-correlated single-photon counting (TCSPC) and multi-channel scaling (MCS) methods, respectively. Average lifetimes are obtained as $\tau_{av} = \frac{\sum A_i \tau_i^2}{\sum A_i \tau_i}$ from bi-exponential fits. Low-temperature measurements were performed by immersion of the sample in a liquid N_2 quartz dewar.

3. Results

3.1. Crystal Structure Characterization

Compound **[Cu_2I_2(TT-Py)]$_n$** (**1**) crystallizes as very thin yellow needles by slow diffusion of acetonitrile solutions of CuI and **TT-Py**. X-ray diffraction analysis shows that it crystallizes in the $P2_1/n$ space group of the monoclinic system to give a monodimensional coordination network. The asymmetric unit contains one ligand molecule, two copper and two iodide atoms, as illustrated in Figure 1. Crystallographic data and selected bond distances and angles are given in Tables S1 and S2, respectively.

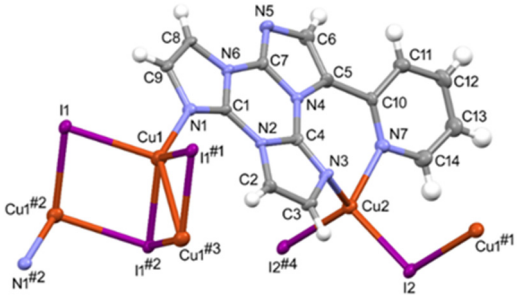

Figure 1. Crystal structure of **1**: portion of the crystal structure showing the coordination spheres of copper(I) atoms, with labelling scheme. Ellipsoids are drawn at 30% probability level. Symmetry codes: (#1): 1 + x, y, z; (#2): −x, −y, −z; (#3): 1 − x, −y, −z; (#4): 1 − x, y, z.

The monodimensional coordination network of **1** is composed of a bridging **TT-Py** ligand and two very common structural motifs for copper(I) halide-based compounds, which are the double-stranded stair and the single zig-zag chain. The double-stranded stair, of composition $[Cu_2I_2]_n$, is built up by distorted tetrahedral Cu1 atoms and μ_3-iodide ions adopting distorted trigonal pyramidal geometry. Cu1, in addition to being bonded to three μ_3-iodide, complets its tetrahedral environment by coordination to one imidazole nitrogen atom of **TT-Py** (N1) (see Figure 1).

Cu-I and Cu-N bond distances are similar to those of other known stairs analogous to that present in **1** [47,48] and, in particular, to that of the strictly related species **[Cu_2I_2(TT)]$_n$**, where the nitrogen ligand is the non-substituted cyclic triimidazole molecule [26,27]. Along the stair of **1**, the Cu1···Cu1 nearest neighbor distances show two different values, namely 3.4134(12) Å and 2.7625(11) Å, which are, respectively, alternately longer and shorter than the sum of van der Waals radii of Cu(I) ions (2.80 Å) [49]. The dihedral angle between adjacent Cu_2I_2 planar units along the stairs is 113.92° (Figure 2). The ligands are disposed on both sides of the stairs with the TT fragments and the pyridine groups all parallel to each other. The distances between triazinic centroids and between pyridine centroids of adjacent ligands are the same and correspond to 4.271 Å (the unit cell parameter *a*). The presence of the 2-pyridine attached to the TT fragment allows the coordination of a second copper atom (Cu2) by N3 (imidazole) and N7 (pyridine) nitrogen atoms belonging to the same ligand, generating a seven-membered chelate ring (Figure 1). To allow the ligand to chelate, the pyridine fragment must rotate around the TT-Py bond, resulting in

a less planar conformation with respect to that found for the free ligand (dihedral angle N7–C10–C5–N4 of 28.60°, to be compared to values in the range 144.4–156.1° found in the different polymorphs of the free ligand [30]). However, the conformation of the chelate ring is very similar to that found in the previously reported compound **[Cu(μ-NO_3)(NO_3)(TT-Py)]**$_n$ [28], in which the ligand chelates in a similar manner (dihedral angle of 28.4°). Cu2 has a [CuI_2N_2] distorted tetrahedral coordination environment, being coordinated by two bridging iodide ions (I2), in addition to the two nitrogen atoms, giving rise to a zig-zag chain of composition [CuI]$_n$. Bridging iodide has an angular geometry and, along the chain, the I···I distance (which is equal to the Cu···Cu distance) is of 4.271 Å (the unit cell parameter *a*). A center of inversion located on the ladder generated a second zig-zag chain with opposite orientation with respect to the central ladder motif. The overall structural motif remains, then, monodimensional, being made by three parallel copper iodide chains connected by bridging ligands.

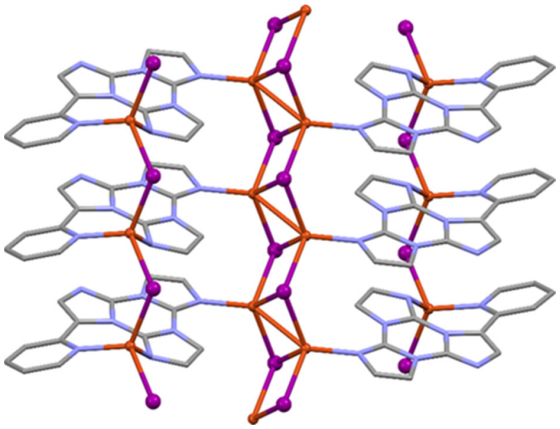

Figure 2. View of a single monodimensional chain of **1**, showing the central double-stranded stair and the two lateral single zig-zag structural motifs bridged by the ligand.

To the best of our knowledge, this structural motif is rare among copper(I) halide-based compounds, and it has been structurally characterized only in the structure of [{Cu(μ_3-I)}$_2$(4,2′-pypzpy)$_2${Cu(μ-I)}$_2$]$_n$ (4,2′-pypzpy = 4-(1-(pyridin-2-yl)-1H-pyrazolyl)pyridine) (CSD refcode GAJBEB [50]), where the ligand is bridging/chelating as **TT-Py**.

The chains are packed, running all in the same direction (the **a** axis) and no significant intermolecular interactions are present between them (Figure 3).

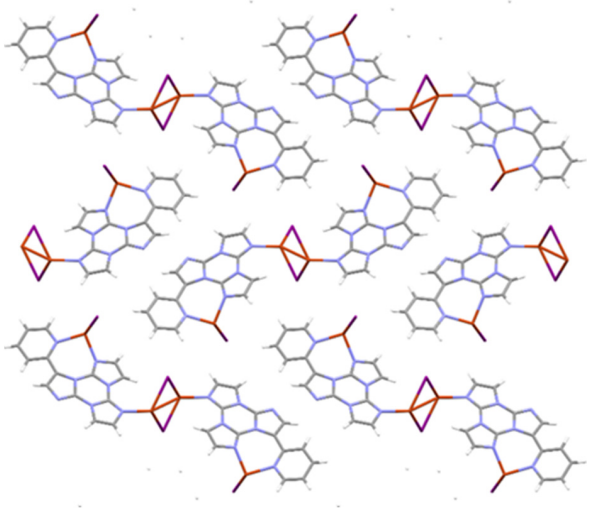

Figure 3. View down the crystallographic axis **a** showing the packing of the monodimensional chains of **1**.

3.2. X-ray Powder Diffraction (XRPD) and Thermal Analysis

The good agreement between the experimental powder diffraction pattern and the one calculated from the X-ray single crystal data (see Figure S1) confirms the obtainment of the bulk sample of **1** as a single pure phase proven to be stable in air and insoluble in common organic solvents. The thermogravimetric analysis (TGA) reveals that **1** is stable up to ca. 305 °C. At this temperature, a weight loss of ca. 41% is observed, corresponding to the loss of one ligand molecule (calculated 42%) (see Figure S2).

3.3. Photophysical Characterization and Theoretical Investigation

Photoluminescence studies on crystalline powders of **1** were performed both at 298 and 77 K. At room temperature, the spectrum is dominated by a broad excitation-independent emission centered at 588 nm (quantum yield, Φ, equal to 7%, τ = 1.33 μs, Figure S3). Spectra collected in the 270–580 nm excitation range show a superimposable emission. The spectrum obtained at 300 nm excitation is reported as an exemplar in Figure 4. Similarly, at 77 K, an excitation-independent long-lived emission centered at 580 nm (τ = 17.89 μs) is observed (Figure 4 and Figure S4). Therefore, the emissive behavior of **1** results to be quite different from that previously observed for **[CuI(TT)]$_n$**, displaying excitation-dependent photoluminescence comprising non-thermally equilibrated XMLCT and ligand-centered emissive states [27]. More precisely, **[CuI(TT)]$_n$** displays an intense and broad phosphorescent band at 568 nm when excited at a high energy (300–360 nm) and two far less intense vibronically resolved long-lived emissions at lower (>390 nm) excitation energies. These two latter components, interpreted as supramolecular contributions associated respectively to the N···I interacting species and π-π stacks of the **TT** ligand, are lacking in **1**.

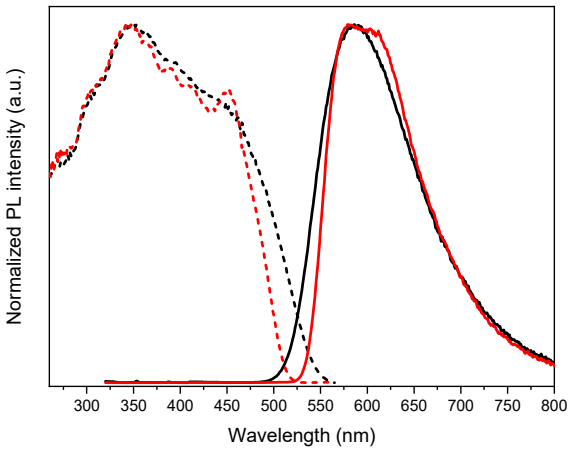

Figure 4. Normalized excitation (dashed) and emission (continuous) spectra of crystalline powders of **1** at 298 K (black, λ_{em} = 588 nm; λ_{exc} = 300 nm) and 77 K (red, λ_{em} = 580 nm; λ_{exc} = 300 nm).

To interpret this different photophysical behavior, DFT and TDDFT calculations were performed on a discrete model of the **[Cu$_2$I$_2$(TT-Py)]$_n$** infinite coordination polymer, using the same computational protocol adopted for the discrete model of **[CuI(TT)]$_n$** [27,29] (see Figures S6 and S7, respectively, for HOMOs and LUMOs plots involved in the low energy transitions; and Tables S4 and S5, respectively, for the singlet and triplet excitation energies and main orbital contributions [51]). It is found that, while for both compounds the LUMOs are distributed only on the ligand, the HOMOs display different delocalization schemes. For the **[Cu$_2$I$_2$(TT-Py)]$_n$** model, *all* the HOMOs are localized on either the CuI inorganic core (related to either the double strand or the single chain) or the CuI-ligand unit (CuI belonging to the double strand). In particular, the former are the high-lying HOMOs and are mainly involved in the high energy triplets, while the latter are inner HOMOs and principally contribute to the low energy triplets (T_1–T_4, see Figure 5). On the other hand, for the **[CuI(TT)]$_n$** model compound, some HOMOs are localized on either the Cu-I inorganic part or the Cu-ligand unit; while, the others are distributed exclusively on the

ligand. Therefore, while for **[CuI(TT)]$_n$**, both MLCT (or XMLCT) and LC transitions are expected, the former associated with the broad phosphorescence band and the latter to the two weaker long-lived components; for **[Cu$_2$I$_2$(TT-Py)]$_n$**, all the low-energy transitions are of MLCT or XMLCT character, reflecting in only one long-lived emission. Such different emissive behavior can be explained by the different coordination scheme in the two CPs: in **[CuI(TT)]$_n$**, the organic ligand coordinates one metal ion only, giving rise to a single Cu-N bond, while in **[Cu$_2$I$_2$(TT-Py)]$_n$**, it coordinates two metal ions, forming three Cu-N bonds; therefore, enhancing the charge delocalization on the whole metal–ligand system.

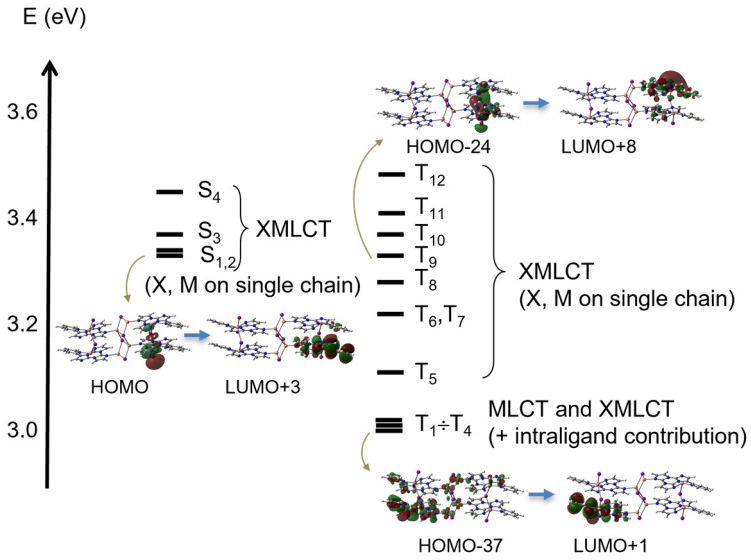

Figure 5. Electronic levels computed for the model compound of **[Cu$_2$I$_2$(TT-Py)]$_n$** and MOs mainly involved in the S_1, T_1 and T_9 transitions [51].

Moreover, based on the observed lifetimes, increasing by one order of magnitude from 298 to 77 K and on the presence of a triplet (T_9, see Figure 5) almost isoenergetic with S_1, a TADF (thermally activated delayed fluorescence) mechanism at the origin of the single emission of **[Cu$_2$I$_2$(TT-Py)]$_n$** cannot be excluded.

4. Conclusions

The coordination ability of the nitrogen-rich derivative of cyclic trimidazole **TT-Py**, bearing a pyridinic substituent on the triazinic scaffold, was exploited for the preparation and structural characterization of a new Cu(I) coordination polymer by reaction in mild conditions with CuI. The new species **[Cu$_2$I$_2$(TT-Py)]$_n$** (**1**) was characterized by single crystal X-ray diffraction, showing a quite rare monodimensional structural motif comprising both the double-stranded stair and the zig-zag chain, which are typical in the Cu(I) halides derivatives. To our knowledge, a similar structure based on a monodentate bridging/chelating ligand was reported only for the CuI compound [{Cu(μ_3-I)}$_2$(4,2′-pypzpy)$_2${Cu(μ-I)}$_2$]$_n$ (4,2′-pypzpy = 4-(1-(pyridin-2-yl)-1H-pyrazolyl)pyridine). The photophysical behavior of **1** in the solid state was investigated and compared to that of the previously reported **[CuI(TT)]$_n$** containing only double-stranded stairs. Interestingly, the two compounds show a different behavior, which was elucidated on the basis of DFT and TDDFT theoretical calculations. In particular, the long-lived emissions observed for **[CuI(TT)]$_n$** at low-excitation energies and associated with the supramolecular contributions given by N···I interacting species and π–π stacks of the TT ligand, are missing in **1**. The main reason for such different emissive behavior is attributed to the different number of Cu-N interactions in the two compounds (one and three Cu-N bonds in **[CuI(TT)]$_n$** and **1**, respectively), allowing an enhanced charge delocalization on the whole metal–ligand system in **1**.

Supplementary Materials: The following supporting information can be downloaded at: https://www.mdpi.com/article/10.3390/cryst13010149/s1, Figures S1 and S2: XRPD patterns and TGA analysis; Figures S3 and S4: Photophysical data; Figure S5: Model compound; Figures S6 and S7: Plots of the molecular orbitals; Tables S1 and S2: Crystal data and selected bond distances and angles; Table S3: Selected optimized bond distances for the model compound; Tables S4 and S5: Computed transitions for the model compound.

Author Contributions: Investigation, D.M. (Daniele Malpicci), D.B. and D.M. (Daniele Marinotto); data curation, D.M. (Daniele Malpicci), D.B., L.C., A.F., E.L., D.M. (Daniele Marinotto) and E.C.; writing, E.L., E.C., A.F. and L.C.; supervision, A.F., E.C. and L.C. All the authors have read and agreed to the published version of the manuscript.

Funding: This research received no external funding.

Data Availability Statement: Not applicable.

Acknowledgments: The use of instrumentation purchased through the Regione Lombardia-Fondazione Cariplo joint SmartMatLab Project is gratefully acknowledged. This work was supported by the University of Milan (Project PSR2021_DIP_005_PI_DCARL).

Conflicts of Interest: The authors declare no conflict of interest.

References and Note

1. Kobayashi, A.; Kato, M. Stimuli-Responsive Luminescent Copper(I) Complexes for Intelligent Emissive Devices. *Chem. Lett.* **2016**, *46*, 154–162. [CrossRef]
2. Czerwieniec, R.; Leitl, M.J.; Homeier, H.H.H.; Yersin, H. Cu(I) Complexes—Thermally Activated Delayed Fluorescence. Photophysical Approach and Material Design. *Coord. Chem. Rev.* **2016**, *325*, 2–28. [CrossRef]
3. Cariati, E.; Lucenti, E.; Botta, C.; Giovanella, U.; Marinotto, D.; Righetto, S. Cu(I) Hybrid Inorganic–Organic Materials with Intriguing Stimuli Responsive and Optoelectronic Properties. *Coord. Chem. Rev.* **2016**, *306*, 566–614. [CrossRef]
4. Tsuge, K.; Chishina, Y.; Hashiguchi, H.; Sasaki, Y.; Kato, M.; Ishizaka, S.; Kitamura, N. Luminescent Copper(I) Complexes with Halogenido-Bridged Dimeric Core. *Coord. Chem. Rev.* **2016**, *306*, 636–651. [CrossRef]
5. Dumur, F. Recent Advances in Organic Light-Emitting Devices Comprising Copper Complexes: A Realistic Approach for Low-Cost and Highly Emissive Devices? *Org. Electron.* **2015**, *21*, 27–39. [CrossRef]
6. Singha, S.; Kim, D.; Seo, H.; Cho, S.W.; Ahn, K.H. Fluorescence Sensing Systems for Gold and Silver Species. *Chem. Soc. Rev.* **2015**, *44*, 4367–4399. [CrossRef]
7. Hamze, R.; Peltier, J.L.; Sylvinson, D.; Jung, M.; Cardenas, J.; Haiges, R.; Soleilhavoup, M.; Jazzar, R.; Djurovich, P.I.; Bertrand, G.; et al. Eliminating Nonradiative Decay in Cu(I) Emitters: >99% Quantum Efficiency and Microsecond Lifetime. *Science* **2019**, *363*, 601–606. [CrossRef]
8. Yam, V.W.-W.; Au, V.K.-M.; Leung, S.Y.-L. Light-Emitting Self-Assembled Materials Based on d^8 and d^{10} Transition Metal Complexes. *Chem. Rev.* **2015**, *115*, 7589–7728. [CrossRef]
9. Xin, X.-L.; Chen, M.; Ai, Y.; Yang, F.; Li, X.-L.; Li, F. Aggregation-Induced Emissive Copper(I) Complexes for Living Cell Imaging. *Inorg. Chem.* **2014**, *53*, 2922–2931. [CrossRef]
10. Wang, S.; Morgan, E.E.; Panuganti, S.; Mao, L.; Vishnoi, P.; Wu, G.; Liu, Q.; Kanatzidis, M.G.; Schaller, R.D.; Seshadri, R. Ligand Control of Structural Diversity in Luminescent Hybrid Copper(I) Iodides. *Chem. Mater.* **2022**, *34*, 3206–3216. [CrossRef]
11. Ford, P.C.; Cariati, E.; Bourassa, J. Photoluminescence Properties of Multinuclear Copper(I) Compounds. *Chem. Rev.* **1999**, *99*, 3625–3647. [CrossRef]
12. Conesa-Egea, J.; Zamora, F.; Amo-Ochoa, P. Perspectives of the Smart Cu-Iodine Coordination Polymers: A Portage to the World of New Nanomaterials and Composites. *Coord. Chem. Rev.* **2019**, *381*, 65–78. [CrossRef]
13. Perruchas, S. Molecular Copper Iodide Clusters: A Distinguishing Family of Mechanochromic Luminescent Compounds. *Dalt. Trans.* **2021**, *50*, 12031–12044. [CrossRef]
14. Schlachter, A.; Viau, L.; Fortin, D.; Knauer, L.; Strohmann, C.; Knorr, M.; Harvey, P.D. Control of Structures and Emission Properties of $(CuI)_n$ 2-Methyldithiane Coordination Polymers. *Inorg. Chem.* **2018**, *57*, 13564–13576. [CrossRef]
15. Troyano, J.; Zapata, E.; Perles, J.; Amo-Ochoa, P.; Fernández-Moreira, V.; Martínez, J.I.; Zamora, F.; Delgado, S. Multifunctional Copper(I) Coordination Polymers with Aromatic Mono- and Ditopic Thioamides. *Inorg. Chem.* **2019**, *58*, 3290–3301. [CrossRef] [PubMed]
16. Troyano, J.; Perles, J.; Amo-Ochoa, P.; Zamora, F.; Delgado, S. Strong Luminescent Copper(I) Halide Coordination Polymers and Dinuclear Complexes with Thioacetamide and N,N′-Donor Ligands. *CrystEngComm* **2016**, *18*, 1809–1817. [CrossRef]
17. Artem'Ev, A.V.; Doronina, E.P.; Rakhmanova, M.I.; Tarasova, O.A.; Bagryanskaya, I.Y.; Nedolya, N.A. Chemoselective Mechanochemical Route toward a Bright TADF-Emitting CuI-Based Coordination Polymer. *Inorg. Chem. Front.* **2019**, *6*, 671–679. [CrossRef]

18. Troyano, J.; Castillo, Ó.; Amo-Ochoa, P.; Martínez, J.I.; Zamora, F.; Delgado, S. Reversible Transformation between Cu(I)-Thiophenolate Coordination Polymers Displaying Luminescence and Electrical Properties. *CrystEngComm* **2019**, *21*, 3232–3239. [CrossRef]
19. Artem'ev, A.V.; Baranov, A.Y.; Rakhmanova, M.I.; Malysheva, S.F.; Samsonenko, D.G. Copper(I) Halide Polymers Derived from Tris [2-(Pyridin-2-Yl)Ethyl]Phosphine: Halogen-Tunable Colorful Luminescence Spanning from Deep Blue to Green. *New J. Chem.* **2020**, *44*, 6916–6922. [CrossRef]
20. Vinogradova, K.A.; Shekhovtsov, N.A.; Berezin, A.S.; Sukhikh, T.S.; Rogovoy, M.I.; Artem'ev, A.V.; Bushuev, M.B. Coordination-Induced Emission Enhancement in Copper(I) Iodide Coordination Polymers Supported by 2-(Alkylsulfanyl)Pyrimidines. *Dalt. Trans.* **2021**, *50*, 9317–9330. [CrossRef]
21. Conesa-Egea, J.; Moreno-Vázquez, A.; Fernández-Moreira, V.; Ballesteros, Y.; Castellanos, M.; Zamora, F.; Amo-Ochoa, P. Micro and Nano Smart Composite Films Based on Copper-Iodine Coordination Polymer as Thermochromic Biocompatible Sensors. *Polymers* **2019**, *11*, 1047. [CrossRef] [PubMed]
22. An, Z.; Zheng, C.; Tao, Y.; Chen, R.; Shi, H.; Chen, T.; Wang, Z.; Li, H.; Deng, R.; Liu, X.; et al. Stabilizing Triplet Excited States for Ultralong Organic Phosphorescence. *Nat. Mater.* **2015**, *14*, 685–690. [CrossRef] [PubMed]
23. Lucenti, E.; Forni, A.; Botta, C.; Carlucci, L.; Giannini, C.; Marinotto, D.; Previtali, A.; Righetto, S.; Cariati, E. H-Aggregates Granting Crystallization-Induced Emissive Behavior and Ultralong Phosphorescence from a Pure Organic Molecule. *J. Phys. Chem. Lett.* **2017**, *8*, 1894–1898. [CrossRef] [PubMed]
24. Cariati, E.; Forni, A.; Lucenti, E.; Marinotto, D.; Previtali, A.; Righetto, S.; Botta, C.; Bold, V.; Kravtsov, V.; Fonari, M.S. Extrinsic Heavy Metal Atom Effect on the Solid-State Room Temperature Phosphorescence of Cyclic Triimidazole. *Chem. Asian J.* **2019**, *14*, 853–858. [CrossRef]
25. Fonari, M.S.; Kravtsov, V.C.; Bold, V.; Lucenti, E.; Cariati, E.; Marinotto, D.; Forni, A. Structural Landscape of Zn(II) and Cd(II) Coordination Compounds with Two Isomeric Triimidazole Luminophores: Impact of Crystal Packing Patterns on Emission Properties. *Cryst. Growth Des.* **2021**, *21*, 4184–4200. [CrossRef]
26. Lucenti, E.; Cariati, E.; Previtali, A.; Marinotto, D.; Forni, A.; Bold, V.; Kravtsov, V.C.; Fonari, M.S.; Galli, S.; Carlucci, L. Versatility of Cyclic Triimidazole to Assemble 1D, 2D, and 3D Cu(I) Halide Coordination Networks. *Cryst. Growth Des.* **2019**, *19*, 1567–1575. [CrossRef]
27. Malpicci, D.; Lucenti, E.; Forni, A.; Marinotto, D.; Previtali, A.; Carlucci, L.; Mercandelli, P.; Botta, C.; Righetto, S.; Cariati, E. Ag(I) and Cu(I) Cyclic-Triimidazole Coordination Polymers: Revealing Different Deactivation Channels for Multiple Room Temperature Phosphorescences. *Inorg. Chem. Front.* **2021**, *8*, 1312–1323. [CrossRef]
28. Melnic, E.; Kravtsov, V.C.; Lucenti, E.; Cariati, E.; Forni, A.; Siminel, N.; Fonari, M.S. Regulation of $\pi\cdots\pi$ Stacking Interactions between Triimidazole Luminophores and Comprehensive Emission Quenching by Coordination to Cu(II). *New J. Chem.* **2021**, *45*, 9040–9052. [CrossRef]
29. Forni, A.; Cariati, E.; Carlucci, L.; Lucenti, E.; Marinotto, D.; Pieraccini, S.; Sironi, M. Interpreting the Different Emissive Properties of Cyclic Triimidazole-Based CuI and AgI Coordination Polymers: A QTAIM and IQA Study. *Acta Cryst. Sect. B Struct. Sci. Cryst. Eng. Mater.* **2021**, *77*, 865–870. [CrossRef]
30. Lucenti, E.; Forni, A.; Previtali, A.; Marinotto, D.; Malpicci, D.; Righetto, S.; Giannini, C.; Virgili, T.; Kabacinski, P.; Ganzer, L.; et al. Unravelling the Intricate Photophysical Behavior of 3-(Pyridin-2-Yl)Triimidazotriazine AIE and RTP Polymorphs. *Chem. Sci.* **2020**, *11*, 7599–7608. [CrossRef]
31. *SADABS 2012. Area Detector Absorption Correction*; Bruker AXS Inc.: Madison, WI, USA, 2012.
32. Burla, M.C.; Caliandro, R.; Carrozzini, B.; Cascarano, G.L.; Cuocci, C.; Giacovazzo, C.; Mallamo, M.; Mazzone, A.; Polidori, G. Crystal Structure Determination and Refinement Via SIR2014. *J. Appl. Cryst.* **2015**, *48*, 306–309. [CrossRef]
33. Sheldrick, G.M. Crystal Structure Refinement with SHELXL. *Acta Cryst. Sect. C Struct. Chem.* **2015**, *71*, 3–8. [CrossRef] [PubMed]
34. Frisch, M.J.; Trucks, G.W.; Schlegel, H.B.; Scuseria, G.E.; Robb, M.A.; Cheeseman, J.R.; Scalmani, G.; Barone, V.; Petersson, G.A.; Nakatsuji, H.; et al. *Gaussian 16 Rev. A.03*; Gaussian: Wallingford, CT, USA, 2016.
35. Pritchard, B.P.; Altarawy, D.; Didier, B.; Gibson, T.D.; Windus, T.L. New Basis Set Exchange: An Open, Up-to-Date Resource for the Molecular Sciences Community. *J. Chem. Inf. Model.* **2019**, *59*, 4814–4820. [CrossRef]
36. Feller, D. The Role of Databases in Support of Computational Chemistry Calculations. *J. Comput. Chem.* **1996**, *17*, 1571–1586. [CrossRef]
37. Schuchardt, K.L.; Didier, B.T.; Elsethagen, T.; Sun, L.; Gurumoorthi, V.; Chase, J.; Li, J.; Windus, T.L. Basis Set Exchange: A Community Database for Computational Sciences. *J. Chem. Inf. Model.* **2007**, *47*, 1045–1052. [CrossRef] [PubMed]
38. Glukhovtsev, M.N.; Pross, A.; McGrath, M.P.; Radom, L. Extension of Gaussian-2 (G2) Theory to Bromine- and Iodine-Containing Molecules: Use of Effective Core Potentials. *J. Chem. Phys.* **1995**, *103*, 1878–1885. [CrossRef]
39. Chai, J.-D.; Head-Gordon, M. Systematic Optimization of Long-Range Corrected Hybrid Density Functionals. *J. Chem. Phys.* **2008**, *128*, 84106. [CrossRef]
40. Malpicci, D.; Giannini, C.; Lucenti, E.; Forni, A.; Marinotto, D.; Cariati, E. Mono-, Di-, Tri-Pyrene Substituted Cyclic Triimidazole: A Family of Highly Emissive and RTP Chromophores. *Photochem* **2021**, *1*, 477–487. [CrossRef]
41. Previtali, A.; He, W.; Forni, A.; Malpicci, D.; Lucenti, E.; Marinotto, D.; Carlucci, L.; Mercandelli, P.; Ortenzi, M.A.; Terraneo, G.; et al. Tunable Linear and Nonlinear Optical Properties from Room Temperature Phosphorescent Cyclic Triimidazole-Pyrene Bio-Probe. *Chem. Eur. J.* **2021**, *27*, 16690–16700. [CrossRef] [PubMed]

42. Previtali, A.; Lucenti, E.; Forni, A.; Mauri, L.; Botta, C.; Giannini, C.; Malpicci, D.; Marinotto, D.; Righetto, S.; Cariati, E. Solid State Room Temperature Dual Phosphorescence from 3-(2-Fluoropyridin-4-Yl)Triimidazo[1,2-*a*:1′,2′-*c*:1″,2″-*e*][1,3,5]Triazine. *Molecules* **2019**, *24*, 2552. [CrossRef]
43. Giannini, C.; Forni, A.; Malpicci, D.; Lucenti, E.; Marinotto, D.; Previtali, A.; Carlucci, L.; Cariati, E. Room Temperature Phosphorescence from Organic Materials: Unravelling the Emissive Behaviour of Chloro-Substituted Derivatives of Cyclic Triimidazole. *Eur. J. Org. Chem.* **2021**, *2021*, 2041–2049. [CrossRef]
44. Lucenti, E.; Forni, A.; Botta, C.; Carlucci, L.; Colombo, A.; Giannini, C.; Marinotto, D.; Previtali, A.; Righetto, S.; Cariati, E. The Effect of Bromo Substituents on the Multifaceted Emissive and Crystal-Packing Features of Cyclic Triimidazole Derivatives. *ChemPhotoChem* **2018**, *2*, 801–805. [CrossRef]
45. Lucenti, E.; Forni, A.; Botta, C.; Carlucci, L.; Giannini, C.; Marinotto, D.; Pavanello, A.; Previtali, A.; Righetto, S.; Cariati, E. Cyclic Triimidazole Derivatives: Intriguing Examples of Multiple Emissions and Ultralong Phosphorescence at Room Temperature. *Angew. Chem. Int. Ed.* **2017**, *56*, 16302–16307. [CrossRef]
46. Lucenti, E.; Forni, A.; Botta, C.; Giannini, C.; Malpicci, D.; Marinotto, D.; Previtali, A.; Righetto, S.; Cariati, E. Intrinsic and Extrinsic Heavy-Atom Effects on the Multifaceted Emissive Behavior of Cyclic Triimidazole. *Chem. Eur. J.* **2019**, *25*, 2452–2456. [CrossRef] [PubMed]
47. Conesa-Egea, J.; Redondo, C.D.; Martínez, J.I.; Gómez-García, C.J.; Castillo, Ó.; Zamora, F.; Amo-Ochoa, P. Supramolecular Interactions Modulating Electrical Conductivity and Nanoprocessing of Copper–Iodine Double-Chain Coordination Polymers. *Inorg. Chem.* **2018**, *57*, 7568–7577. [CrossRef]
48. Hassanein, K.; Conesa-Egea, J.; Delgado, S.; Castillo, O.; Benmansour, S.; Martínez, J.I.; Abellán, G.; Gómez-García, C.J.; Zamora, F.; Amo-Ochoa, P. Electrical Conductivity and Strong Luminescence in Copper Iodide Double Chains with Isonicotinato Derivatives. *Chem. Eur. J.* **2015**, *21*, 17282–17292. [CrossRef]
49. Shannon, R.D. Revised Effective Ionic Radii and Systematic Studies of Interatomic Distances in Halides and Chalcogenides. *Acta Cryst. Sect. A* **1976**, *32*, 751–767. [CrossRef]
50. Li, J.-C.; Li, H.-X.; Li, H.-Y.; Gong, W.-J.; Lang, J.-P. Ligand Coordination Site-Directed Assembly of Copper(I) Iodide Complexes of ((Pyridyl)-1-Pyrazolyl)Pyridine. *Cryst. Growth Des.* **2016**, *16*, 1617–1625. [CrossRef]
51. It should be noted that geometry optimization of discrete models implies a loss of the symmetry characterizing the polymeric structure owing to major boundary effects, giving rise to an artificial splitting of the electronic excitation levels.

Disclaimer/Publisher's Note: The statements, opinions and data contained in all publications are solely those of the individual author(s) and contributor(s) and not of MDPI and/or the editor(s). MDPI and/or the editor(s) disclaim responsibility for any injury to people or property resulting from any ideas, methods, instructions or products referred to in the content.